Inorganic Chemistry

Article

pubs.acs.org/IC

One Electron Reduced Square Planar Bis(benzene-1,2-dithiolato) Copper Dianionic Complex and Redox Switch by O_2/HO^-

Biplab K. Maiti,[†] Luisa B. Maia,[†] Kuntal Pal,[‡] Bholanath Pakhira,[§] Teresa Avilés,*[,†,⊥] Isabel Moura,[†] Sofia R. Pauleta,[†] José L. Nuñez,[∥] Alberto C. Rizzi,[∥] Carlos D. Brondino,*[,∥] Sabyasachi Sarkar,*[,§] and José J. G. Moura*[,†]

[†]UCIBIO@REQUIMTE, Departamento de Química, FCT, Universidade Nova de Lisboa, 2829-516 Caparica, Portugal

[‡]School of Chemistry, The University of Manchester, Manchester, M13 9PL, U.K.

[§]Department of Chemistry, Indian Institute of Engineering Science and Technology, Shibpur, Botanic Garden, Howrah 711103, West Bengal, India

[∥]Departamento de Física, Facultad de Bioquímica y Ciencias Biológicas, Universidad Nacional del Litoral, Ciudad Universitaria, Paraje El Pozo, S3000ZAA Santa Fe, Argentina

Supporting Information

ABSTRACT: The complex $[Ph_4P]_2[Cu(bdt)_2]$ ($\mathbf{1}^{red}$) was synthesized by the reaction of $[Ph_4P]_2[S_2MoS_2CuCl]$ with H_2bdt (bdt = benzene-1,2-dithiolate) in basic medium. $\mathbf{1}^{red}$ is highly susceptible toward dioxygen, affording the one electron oxidized diamagnetic compound $[Ph_4P][Cu(bdt)_2]$ ($\mathbf{1}^{ox}$). The interconversion between these two oxidation states can be switched by addition of O_2 or base (Et_4NOH = tetraethylammonium hydroxide), as demonstrated by cyclic voltammetry and UV−visible and EPR spectroscopies. Thiomolybdates, in free or complex forms with copper ions, play an important role in the stability of $\mathbf{1}^{red}$ during its synthesis, since in its absence, $\mathbf{1}^{ox}$ is isolated. Both $\mathbf{1}^{red}$ and $\mathbf{1}^{ox}$ were structurally characterized by X-ray crystallography. EPR experiments showed that $\mathbf{1}^{red}$ is a Cu(II)−sulfur complex and revealed strong covalency on the copper−sulfur bonds. DFT calculations confirmed the spin density delocalization over the four sulfur atoms (76%) and copper (24%) atom, suggesting that $\mathbf{1}^{red}$ has a "thiyl radical character". Time dependent DFT calculations identified such ligand to ligand charge transfer transitions. Accordingly, $\mathbf{1}^{red}$ is better described by the two isoelectronic structures $[Cu^{I}(bdt_2, 4S^{3-,*})]^{2-} \leftrightarrow [Cu^{II}(bdt_2, 4S^{4-})]^{2-}$. On thermodynamic grounds, oxidation of $\mathbf{1}^{red}$ (doublet state) leads to $\mathbf{1}^{ox}$ singlet state, $[Cu^{III}(bdt_2, 4S^{4-})]^{1-}$.

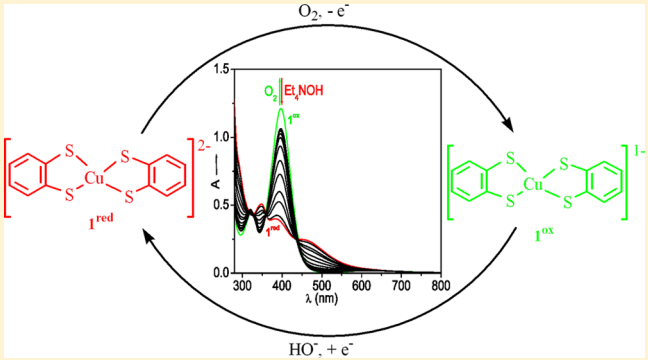

INTRODUCTION

Square planar bis(benzene-1,2-dithiolato (=bdt)) metal complexes have been known since almost half a century ago. Since then, a rich chemistry of transition-metal compounds with benzene-1,2-dithiolato ligands has been developed due to their interesting and unusual electronic properties for potential multielectron storage systems to be used in photochemical or electrochemical splitting of the water molecule and also in bioinorganic chemistry where compounds containing dithiolene ligands are recognized in Mo and W enzymes.[1−6] One of these metal complexes, the diamagnetic monoanion $[Cu(bdt)_2]^{1-}$, was first reported by Gray and co-workers in 1965.[2] Two decades later, Sawyer's group[5] described that the related $[Cu(toluene\text{-}3,4\text{-}dithiolate)_2]^{1-}$ compound possesses two unpaired electrons, one from Cu(II) and the other from the ligand, which remain antiferromagnetically coupled. In 2005, Wieghardt and co-workers ruled out the above conclusion and assigned the electronic structure of such complexes as Cu(III)−thiolate species instead of Cu(II)-thiyl-radical by applying broken symmetry density functional theory (DFT).[6] Extensive structural and spectroscopic data exist in support of the Cu(III)−thiolate complex, but the chemical properties, as well as the electronic structure of the corresponding one electron reduced form of $[Cu(bdt)_2]^{1-}$, are still elusive. Detailed electrochemical studies, used to probe the switching behavior between these two oxidation states, were not conclusive, and an ambiguity remains about which orbital (metal or ligand based atom) is reached by the transferred electron. We unexpectedly succeeded in synthesizing a complex with the formulation $[Ph_4P]_2[Cu(bdt)_2]$ in the solid state, with cation and metal ratio as 2:1, indicating the isolation of the reduced form of the complex. We present here the synthesis, X-ray structure, and electrochemical and spectroscopic properties of $\mathbf{1}^{red}$ (red = reduced form) and of its oxidation product, $\mathbf{1}^{ox}$ (ox = oxidized form), with emphasis on the covalency of Cu−S bonds. We

Received: July 19, 2014
Published: December 3, 2014

also investigated how the interconversion between these two redox states is controlled by O_2 and Et_4NOH (tetraethylammonium hydroxide). The electronic structures of both $\mathbf{1}^{red}$ and $\mathbf{1}^{ox}$ and the $\mathbf{1}^{red} \leftrightarrow \mathbf{1}^{ox}$ redox transition were also characterized using density functional theory (DFT) and time dependent density functional theory (TD-DFT) calculations, which demonstrated that the oxidation process occurs mainly at the sulfur atoms, rather than being a metal based oxidation reaction.

EXPERIMENTAL SECTION

General Consideration. All starting materials were purchased from commercial sources and used without further purification. Solvents were freshly distilled over appropriate drying reagents. The compound $[Ph_4P]_2[S_2MoS_2CuCl]$ was prepared by the literature procedure.[7] Elemental analyses for carbon, hydrogen, nitrogen, and sulfur were recorded with a PerkinElmer 2400 microanalyser. Absorption spectroscopic measurements were performed on a UV-1800 Shimadzu spectrometer. Cyclic voltammetric measurements were made with a BASi Epsilon-EC Bioanalytical Systems, Inc., instrument. Cyclic voltammograms of 10^{-3} M solution of the compound **1** were recorded with a glassy carbon electrode as working electrode, 0.2 M Bu_4NClO_4 as supporting electrolyte, Ag/AgCl electrode as reference electrode, and a platinum auxiliary electrode. The electrochemical experiment was performed under an argon atmosphere at 298 K. Potentials are referenced against internal ferrocene (Fc) and are reported relatively to SHE (standard hydrogen electrode).

Synthesis of $[Ph_4P]_2[Cu(bdt)_2]$ ($\mathbf{1}^{red}$). *Method 1.* A solution of 110 mg (0.1 mmol) of $[Ph_4P]_2[S_2MoS_2CuCl]$ in 20 mL of DMF was treated with 28 mg (0.2 mmol) of benzene-1,2-dithiol (H_2bdt) with 0.4 mmol of Et_4NOH (~0.16 mL of Et_4NOH in 35% water solution). The reaction solution was stirred for 10 min, until a darker brown color formed. After that, the solution was filtered, and the filtrate was layered with 25 mL of Et_2O to afford dark red crystals. The crystals were washed with CH_3CN, ^iPrOH, and Et_2O and finally dried under vacuum. The yield was 57 mg (56%) (Note: In the presence of one equivalent of 1,2-benzenedithiol the same compound was obtained but with lower yield). Anal. Calcd for $C_{60}H_{48}P_2S_4Cu$, M_r = 1022.75: C, 70.39; H, 4.69; S, 12.51. Found: C, 70.41; H, 3.80; S, 12.62. UV/vis: λ_{max} = 348 nm (ε = 9885 M^{-1} cm^{-1}), λ_{max} = 390 nm (ε = 8510 M^{-1} cm^{-1}), and λ_{max} = 472 nm (ε = 4475 M^{-1} cm^{-1}).

Method 2. A solution of 100 mg (0.1 mmol) of $[Ph_4P]_2[MoS_4]$ in 20 mL of DMF was treated with 17 mg (0.1 mmol) of $CuCl_2 \cdot 2H_2O$ and 28 mg (0.2 mmol) of benzene-1,2-dithiol (H_2bdt) with 0.4 mmol of Et_4NOH (~0.16 mL of Et_4NOH in 35% water solution). The reaction solution was stirred for 10 min, until a darker brown color formed. After that, the solution was filtered, and the filtrate was layered with 25 mL of Et_2O to afford dark red crystals ($\mathbf{1}^{red}$). The crystals were washed with CH_3CN, ^iPrOH, and Et_2O and finally dried under vacuum. The yield was 63 mg (62%).

Synthesis of $[Ph_4P][Cu(bdt)_2]$ ($\mathbf{1}^{ox}$).[4] *Method 1.* Compound $\mathbf{1}^{red}$ (102 mg, 0.1 mmol) was dissolved in 80 mL of an air saturated acetonitrile solution at room temperature, and the color of the solution rapidly changed from red to green; it was allowed to evaporate to dryness, leaving green crystals, the $\mathbf{1}^{ox}$. The crystals were washed with ^iPrOH and Et_2O and finally dried under vacuum. The yield was 44 mg (70%).

Method 2. $(Ph_3P)_3CuCl$ (98 mg, 0.1 mmol) was dissolved in 20 mL of DMF and treated with benzene-1,2-dithiol (H_2bdt) (28 mg, 0.2 mmol) and Et_4NOH (0.4 mmol, ~0.16 mL of Et_4NOH in 35% water solution) and with Ph_4PBr (40 mg, 0.1 mmol). The color of the solution changed immediately from the initial red to green; it was then stirred for 10 mi; after that, the solution was filtered, and the filtrate was layered with 30 mL of Et_2O to afford green crystals ($\mathbf{1}^{ox}$). The crystals were washed with ^iPrOH, Et_2O and finally dried under vacuum. The yield was 48 mg (76%).

Crystallography. Suitable diffraction quality crystals of both the complexes were selected and covered with silicon oil to prevent any oxidation during X-ray exposure. X-ray data were collected on a Bruker SMART APEX CCD-based X-ray diffractometer equipped with a CCD area detector. Data were collected using graphite-monochromated Mo Kα radiation (λ = 0.71073 Å) at low temperature (100 K). All empirical absorption corrections were applied using the SADABS program.[8] Cell constants were obtained from the least-squares refinement of three-dimensional centroids through the use of CCD recording of narrow ω rotation frames, completing almost all-reciprocal space in the stated θ range. All data were collected with SMART 5.628 (Bruker, 2003) and were integrated with the Bruker SAINT program. Each structure was solved using SHELXL-97.[9] The space group of each compound was determined based on the lack of systematic absences and intensity statistics. Full-matrix least-squares/difference and Fourier cycles were performed to locate the remaining non-hydrogen atoms. All non-hydrogen atoms were refined with anisotropic displacement parameters. Additional crystallographic calculations were performed with the PLATON[10] program suite. The crystallographic data and refinement parameters are provided in Table 1.

Table 1. Crystallographic Data[b] for $\mathbf{1}^{red}$ and $\mathbf{1}^{ox}$

	$\mathbf{1}^{red}$	$\mathbf{1}^{ox a}$
formula	$C_{60}H_{48}P_2S_4Cu$	$C_{36}H_{28}P_1S_4Cu$
formula wt	1022.75	683.38
cryst syst	monoclinic	monoclinic
space group	$P21/c$	$C2/c$
T [K]	100(2)	100(2)
Z	2	4
a [Å]	11.1360(2)	15.9189(3)
b [Å]	14.7811(3)	11.8882(3)
c [Å]	14.9453(3)	16.5842(3)
α [deg]	90	90
β [deg]	95.013(1)	97.180(1)
γ [deg]	90	90
vol [Å^3]	2450.62(8)	3113.90(11)
D_{calcd} [g cm^{-3}]	1.386	1.458
μ [mm^{-1}]	0.772	1.047
θ range [deg]	2.00−29.18	2.00−28.32
GOF (F_2)	1.060	1.162
wR2[d]	0.1296	0.1197
R1[c]	0.0469	0.0378

[a] See ref 4. [b] Mo Kα radiation (0.71073 Å). [c] $R1 = \sum||F_o| - |F_c||/\sum|F_o|$. [d] $wR2 = \{\sum[w(F_o^2 - F_c^2)^2]/\sum[w(F_o^2)^2]\}^{1/2}$.

EPR Measurements. Powder and frozen solution X-band (9.65 GHz) EPR spectra were recorded using a Bruker EMX 6/1 spectrometer. For 298 K spectra, an ER 4102ST cavity (Bruker) was used. For low-temperature (20 to 120 K) spectra, an ER4116DM rectangular cavity (Bruker) was used and the samples were cooled with helium in an Oxford Instruments ESR900 continuous-flow cryostat, fitted with a temperature controller. The acquisition conditions were a modulation frequency of 100 kHz, modulation amplitude of 0.2 mT, and microwave power of 635 μW. The EPR spectra were simulated with WinEPR SimFonia (ver. 1.25) program from Bruker Analytische GmbH, considering the Hamiltonian

$$\hat{H}_{spin} = \mu_B \hat{S} g B + \hat{I} A \hat{S}$$

where the first and second terms represent the Zeeman and nuclear hyperfine interactions, respectively; $\hat{S}$ is the electron spin angular moment operator, $\hat{I}$, the nuclear spin angular moment operator, A, the nuclear hyperfine interaction constant tensor, μ_B (= 9.274 0154 (31) × 10^{-24} J T^{-1}), the Bohr magneton, and B, the magnetic field. g and A were considered collinear.

Oriented single crystal EPR experiments of $\mathbf{1}^{red}$ at X- and Q-bands were performed on a Bruker EMXplus spectrometer as explained elsewhere.[11] A single crystal of $\mathbf{1}^{red}$ was oriented by gluing its (101)

dx.doi.org/10.1021/ic501742j | Inorg. Chem. 2014, 53, 12799−12808

Scheme 1. Synthesis of 1^{red} (Inside the Box) and Possible Reaction Routes (Outside the Box)[a]

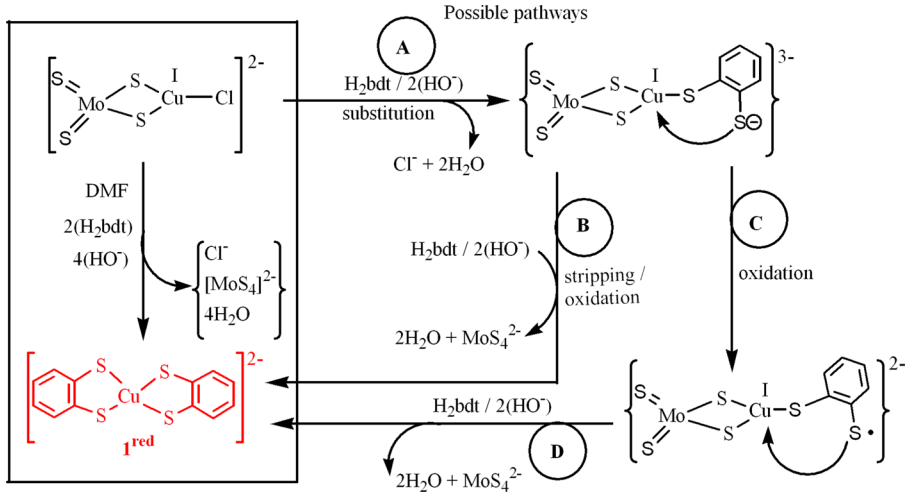

[a]Step A: The reaction between $[MoS_4CuCl]^{2-}$ and 1 equiv of bdt^{2-} ligand to form an intermediate species. Step B: The intermediate uncoordinated sulfur is susceptible to bind to the copper center and simultaneously oxidize and reacts with another equivalent of bdt^{2-} ligand, with release of $[MoS_4]^{2-}$, to produce $\mathbf{1}^{red}$ compound. Step C: Alternatively the intermediate uncoordinated sulfur is oxidized to produce first a thiyl radical species. Step D: Finally this thiyl radical species can react with another equivalent of bdt^{2-} ligand with release of $[MoS_4]^{2-}$ to yield $\mathbf{1}^{red}$. Counter cations are omitted for simplicity.

face to a cleaved KCl cubic holder, which defined a set of orthogonal *xyz* laboratory axes with the *y* direction corresponding to the crystal *b* axis. Additional experimental details are given in the Supporting Information.

DFT and TD-DFT Calculations. All calculations were performed with the Gaussian 03 package (revision B.04).[12] Molecular orbitals were visualized using Gauss View. Geometry optimizations, single point calculations, and population analysis of the molecular orbitals were carried out at the density functional theory (DFT) level with Becke's three parameter hybrid exchange functional,[13] the nonlocal correlation provided by the Lee, Yang, and Parr expression, and the Vosko, Wilk, and Nusair 1980 correlation functional (III) local (B3LYP) 6-31G*+ basis set[14] were used for H, C, N, O, and S atoms. The LANL2DZ[15] basis set and LANL2DZ pseudopotentials of Hay and Wadt[16] were used for the Cu atom. The initial geometry of the anions was taken from the crystal structure, and geometry was optimized without any symmetry constraints. The optimized minima were characterized by harmonic vibration frequency calculations, where minima have no imaginary frequency. For the selected frontier molecular orbitals, their Mulliken spin density populations were calculated in the gas phase (see Figure 8). Open shell and restricted open shell calculations have been carried out to understand the electronic structure. The assignment of the type of each MO was made on the basis of its composition and by visual inspection of its localized orbital. Molecules were optimized on default orientation used by the program and without any symmetry constrained. Additional single point calculations were performed choosing the coordinate frame as *x* and *y* axes are along Cu−S bond and *z* axis along the direction perpendicular to molecular plane. Solvent correction on gas phase free energy has been employed using the same method and basis set, and the conductor like screening model[17] (COSMO). The solvent was chosen as DMF. TD-DFT calculations were carried out using the same basis set with the CPCM model, using DMF as the solvent. Time dependent density functional theory (TD-DFT) calculations were carried out using same basis set with the CPCM model using DMF as the solvent. Singlet excited states were calculated based on the singlet ground-state geometry. The lowest 40 singlet excited states with oscillator strengths greater than 0.01 were considered for TD-DFT calculations, and the singlet excited states were fitted to Gaussian line shapes. The simulated spectra were prepared by fitting each excited state energy to a Gaussian curve with a full width at half-maximum obtained from the experimental spectra.

Calculation of Reduction Potential. Standard one electron reduction potentials for the reduction of A to A^-, $E°$, in solution can be expressed as $\Delta G(\mathrm{Sol}) = -nFE°$, where F is the Faraday constant and n the number of electrons. According to the literature,[18] the reduction potential against standard hydrogen electrode (SHE) can be calculated as $E°_{rel} = -\Delta G(\mathrm{Sol}) - 4.43$ V.

RESULTS AND DISCUSSION

Synthesis. The complex $\mathbf{1}^{red}$ was obtained by the reaction of $[Ph_4P]_2[S_2MoS_2CuCl]$ with H_2bdt in the presence of Et_4NOH as a base, in *N*,*N*-dimethylformamide (DMF) solvent. Our initial aim was to create a model compound[19] for the unique center of the Orange Protein (ORP).[20] So, our attempt was to bind the bdt ligand to a copper center by replacing chloride ion in $[Ph_4P]_2[S_2MoS_2CuCl]$. Unexpectedly, we obtained the product $\mathbf{1}^{red}$, where the $[MoS_4]^{2-}$ moiety is uncoordinated to copper (Scheme 1). Recently, it has been reported that an analogous core containing tungsten, $\{WS_2Cu\}$, reacts with the bdt ligand to produce a structurally characterized $\{WS_2Cu(bdt)\}$ core containing a stable dangling thiyl radical.[21] The reactivity of molybdenum in the present case differs from the tungsten system, due to the relative kinetic instability of molybdenum complex. It is to be noted here that there are differences in the redox stability of thiometalates of Mo and W and, furthermore, the tetrathiometalate is more prone to respond to electron transfer reactions compared with the corresponding dioxodithiometalates. Based on these it was observed that under identical condition when thiotungstate was allowed to react, the copper−tungstate bridged species remain intact with the coordination of bdt on copper uniquely.[21] This did not happen here in the present case, but copper is detached to molybdenum and itself is attached to bdt to provide the reduced species. Here the reducing capability of thiomolybdate acts unlike thiotungsten compound. The reducing capability of thiomolybdate is not straightforward. It scavenges oxygen or other oxidizing agent in a unique way, by an induced electron transfer reaction.[22] The possible intermediate formed here, similar to the reaction with dioxothiotungstate, should be susceptible to redox reaction across the $\{S_2MoS_2Cu\}$ core,

dx.doi.org/10.1021/ic501742j | Inorg. Chem. 2014, 53, 12799−12808

resulting in cleavage of the thiomolybdate part from the isolated $\mathbf{1}^{red}$ product. To understand the role of $\{MoS_4\}$ moiety in the reaction process, we reacted $(PPh_3)_3Cu^{I}Cl$ directly with H_2bdt in the presence of base. This reaction yielded the stable oxidized green compound, $[Ph_4P][Cu^{III}(bdt)_2]$ ($\mathbf{1}^{ox}$),[4] instead of the red colored reduced complex, $\mathbf{1}^{red}$. In contrast, when we used a mixture of $CuCl_2$ and $[Ph_4P]_2[MoS_4]$ or $[Ph_4P]_2[S_2MoS_2CuCl]$ as the starting material, the presence of $\{MoS_4\}$ moiety, either in the form of a separate entity in the reaction mixture or complexed to copper, prevents the copper oxidation and only $\mathbf{1}^{red}$ is successfully isolated (Scheme 2). This

Scheme 2. Synthesis of $\mathbf{1}^{red}$ and $\mathbf{1}^{ox}$[a]

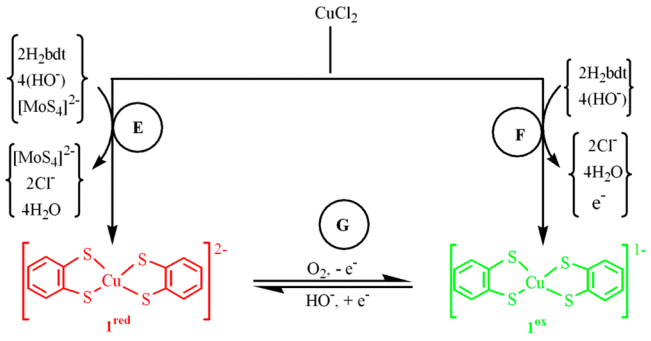

[a]Step E: Cu(II) binds 2 equiv of bdt^{2-} ligand in the presence of $[MoS_4]^{2-}$ to afford compound $\mathbf{1}^{red}$, where $[MoS_4]^{2-}$ does not participate directly in this reaction, but prevents copper oxidation. Step F: Alternatively, Cu(II) binds 2 equiv of bdt^{2-} ligand, without $[MoS_4]^{2-}$, to afford oxidized compound $\mathbf{1}^{ox}$. Step G: The interconversion between these two oxidation states can be switched by addition of O_2 or base Et_4NOH. Counter cations are omitted for simplicity.

suggests that the presence of thiomolybdate in the reaction mixture thwarts the oxidation of copper during the formation of the complex, retaining it in the $\mathbf{1}^{red}$ form (which was further confirmed by the UV–visible titrations discussed below). The compound $\mathbf{1}^{red}$ is stable in the solid state, but it is very susceptible to oxidation in solution, even in the presence of trace amounts of dioxygen. Compound $\mathbf{1}^{red}$ is moderately soluble in acetonitrile or in DMF solvent. A fresh solution of $\mathbf{1}^{red}$ in acetonitrile imparts a red color that under air changes immediately to green, and on evaporation of the solvent, the green crystalline $\mathbf{1}^{ox}$ is isolated.[4]

X-ray Structure. The X-ray crystal structure of $\mathbf{1}^{red}$ (Figure 1) displayed a $\{CuS_4\}$ square-planar core similar to that of $\mathbf{1}^{ox}$. The reduction of $\mathbf{1}^{ox}$ increases the Cu–S bond lengths (d_{Cu-S} = 2.178 ± 0.003 Å for $\mathbf{1}^{ox}$, and d_{Cu-S} = 2.264–2.294 Å for $\mathbf{1}^{red}$)[3,4] as expected. No significant disorder of C–C or C–S bond

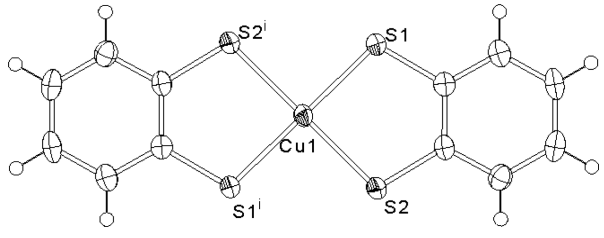

Figure 1. Thermal ellipsoid (50%) drawing of the anion $[Cu(bdt)_2]^{2-}$ ($\mathbf{1}^{red}$). Selected bond distances (Å) are as follows: Cu1–S1 = 2.265 and Cu1–S2 = 2.294.

distance in bdt ligands in $\mathbf{1}^{red}$ or $\mathbf{1}^{ox}$ was observed (Figure 2). The 2-fold-symmetry structure and the contraction of the Cu–

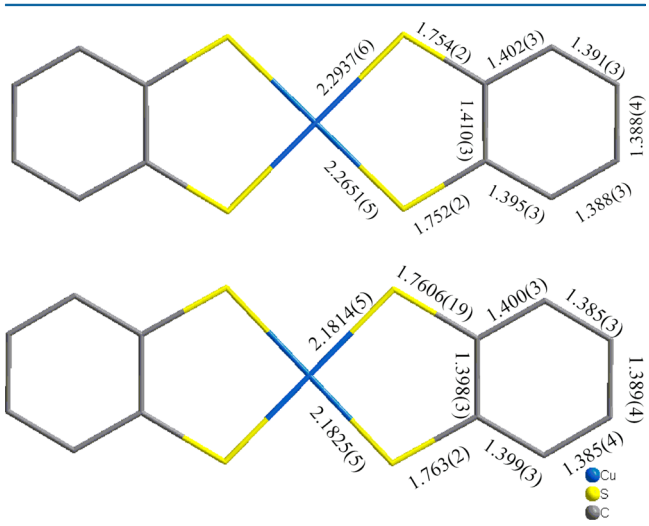

Figure 2. Structure of the respective anions (diamond view) of $\mathbf{1}^{red}$ (top) and $\mathbf{1}^{ox}$ (bottom) with selected bond distance (Å).

S bond distance upon oxidation of $\mathbf{1}^{red}$ suggest that the oxidation could have taken place either on the metal center or on the whole molecule.[23] Hence, based only on the X-ray data, it is not possible to know where the oxidation occurs, if at the copper center or on the $\{Cu–S_4\}$ core. To assign the oxidation state of both the copper and the sulfur atoms in compound $\mathbf{1}^{red}$, EPR spectroscopic studies were further carried out (see below).

Electronic Absorption Spectroscopy. The UV–visible spectrum of $\mathbf{1}^{red}$ in DMF (Figure 3A (inset)) shows well-defined absorption bands at 348 (ε = 9885 M^{-1} cm^{-1}), 390 (ε = 8510 M^{-1} cm^{-1}), and 472 nm (ε = 4475 M^{-1} cm^{-1}). The 348 and 472 nm bands disappeared upon oxidation of $\mathbf{1}^{red}$ to $\mathbf{1}^{ox}$, and two new bands appeared at 320 nm (ε = 9120 M^{-1} cm^{-1}) and 625 nm (ε = 380 M^{-1} cm^{-1}) (Figure 3A). In the presence of dioxygen, the oxidation of $\mathbf{1}^{red}$ led to the enhancement of the intensity of the electronic absorption band at 398 nm (ε = 24120 M^{-1} cm^{-1}), characteristic of the formation of $\mathbf{1}^{ox}$. Curiously, the addition of fresh Et_4NOH to this oxidized solution led to the recovery of the initial spectrum, suggesting the re-formation of $\mathbf{1}^{red}$. The interconversion between $\mathbf{1}^{red}$ and $\mathbf{1}^{ox}$ occurred by the reaction with O_2 (open atmosphere) and Et_4NOH, (4 μL, 35% in water), respectively, as monitored spectroscopically (Figure 3A). Moreover, electronic spectral changes in this interconversion show two isosbestic points; one is tight at 356 nm and other is not so tight at 430 nm, suggesting that such conversion may be either reversible or passing through a common transition state, which was confirmed by the electrochemical studies (see Cyclic Voltammetry). The Et_4NOH destabilizes the electronic state of $\mathbf{1}^{ox}$, but no longer stabilizes the $\mathbf{1}^{red}$ under O_2. In contrast, tetrathiomolybdate, present as $[Ph_4P]_2[MoS_4]$, acts as an oxygen scavenger, preventing oxidation of the copper center in $\mathbf{1}^{red}$ for a long time by using induced electron transfer reaction[22] involving sulfide and thiol as coligand, and it was monitored by electronic spectroscopy (see Supporting Information) and also as had been observed in the $\mathbf{1}^{red}$ synthesis. Bases like Et_3N and even 1,2-benzenedithiol in Et_3N do not show this kind of redox reaction, indicating that only Et_4NOH induces the reduction of copper.

dx.doi.org/10.1021/ic501742j | Inorg. Chem. 2014, 53, 12799–12808

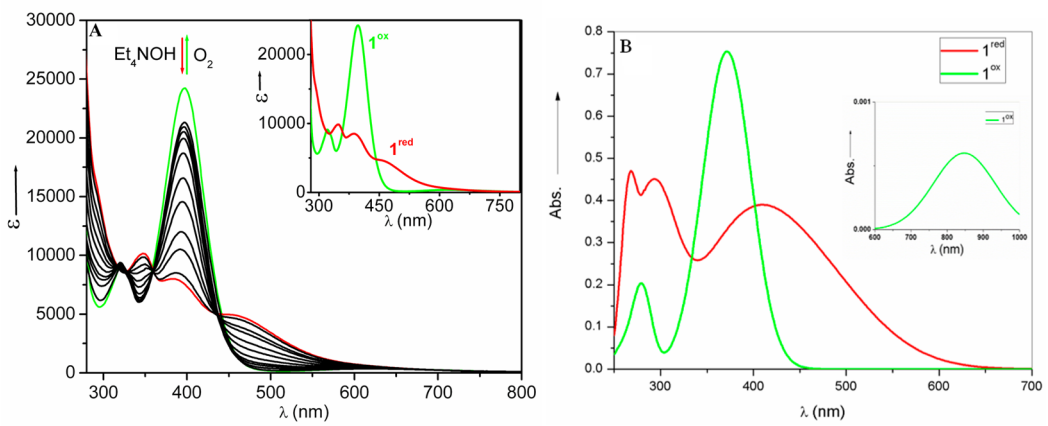

Figure 3. (A) Interconversion between $\mathbf{1}^{red}$ and $\mathbf{1}^{ox}$ in DMF (0.5×10^{-4} M) followed by UV−visible spectroscopy. $\mathbf{1}^{ox}$ spectrum (green) immediately converts into the $\mathbf{1}^{red}$ spectrum (red) by addition of Et_4NOH (4 μL (35% in water) in 10 mL of solution of $\mathbf{1}^{ox}$), and the $\mathbf{1}^{red}$ spectrum reverts to $\mathbf{1}^{ox}$ in the presence of O_2. Spectra were recorded every 1 min. Inset: UV−vis spectra of $\mathbf{1}^{red}$ (red) and $\mathbf{1}^{ox}$ (green). (B) TD-DFT simulated electronic spectra of $\mathbf{1}^{ox}$ and $\mathbf{1}^{red}$ (inset: $\mathbf{1}^{ox}$, dd transition). The vertical transitions are fitted in the Gaussian curve using fwhm from each experimental absorption.

Cyclic Voltammetry. Cyclic voltammetry (CV) was applied to further characterize the redox process responsible for the interconversion between $\mathbf{1}^{red}$ and $\mathbf{1}^{ox}$. In a typical cyclic voltammogram of $\mathbf{1}^{red}$ (Figure 4A), one reversible peak is displayed at $E_{1/2}$ = −0.36 V vs SHE (standard hydrogen electrode) (ΔE_p = 60 mV). Similar voltammograms were observed for $\mathbf{1}^{ox}$. The reversible peak is assigned to the one electron redox couple, $[Cu(bdt)_2]^{1-}/[Cu(bdt)_2]^{2-}$.[6] In the oxidative sweep (red trace) a peak appeared at +0.33 V which influenced the shape of the relevant E_{pc} around −0.39 V, and this is not present under reductive scan (black trace) when the expected sulfur based oxidation has not been reached. The interconversion between the two oxidation states was also observed by CV experiments. Upon addition of Et_4NOH to $\mathbf{1}^{ox}$, the green color immediately changed to red and the reduction potential peak position at −0.36 V was observed (Figure 4B), suggesting that $\mathbf{1}^{red}$ was formed. Further in Figure 4B, the additional peak at +0.33 V responds to the addition of more hydroxide, Et_4NOH (>10 μL (35% in water)), and finally vanishes with the appearance of the new peak at +0.13 V vs SHE; along with this, there is a slight change in the current height of the reversible peak at −0.36 V. Assuming the dilution of the solution due to the addition of hydroxide (which may lead to reduce the current height), its drop is not parallel with the dilution effect, resulting in the disappearance of the peak at +0.33 V. Nevertheless, the reversibility of the main species remained, suggesting that HO^- is only temporarily coordinated to the copper complex. The formation of any other redox species from the reaction with HO^- was excluded, since there is no evidence for its presence within the potential window scanned and there is no effect on the redox state of the compound formed. The new irreversible peak at +0.13 mV vs SHE could be due to an electroactive intermediate species (hydroxide complex). Conversely, the exposure of the assay mixture containing $\mathbf{1}^{red}$ to air changed the solution color to green, but the reduction potential peak position at −0.36 V was maintained.

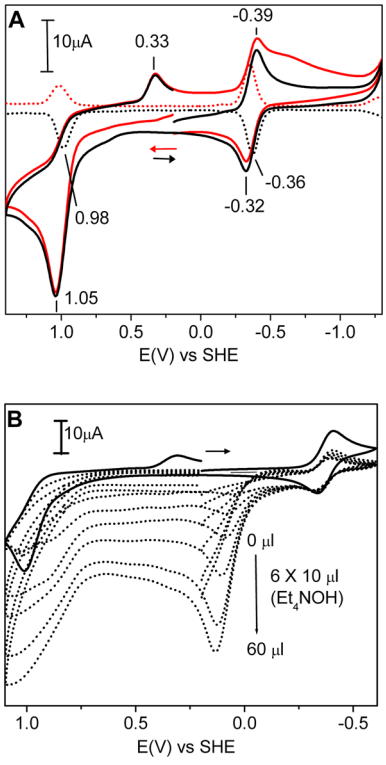

Figure 4. (A) CV (solid lines) and DPP (differential plus polarography) (broken lines) of $\mathbf{1}^{red}$ (1×10^{-3} M) and (B) CV of $\mathbf{1}^{ox}$ (1×10^{-3} M) (solid line) and $\mathbf{1}^{ox}$ with Et_4NOH (35% in water; addition of 10 μL of Et_4NOH each step up to 60 μL; broken lines) in DMF at 298 K were recorded at a scan rate of 100 mV s^{-1} with 0.2 M Bu_4NClO_4 as supporting electrolyte and glassy carbon (GC) as working electrode at room temperature; arrows (red arrow = positive and black arrow = negative) indicate the directions of CV.

Putting together UV−visible titrations and CV experiments, it was demonstrated that $\mathbf{1}^{red}$ and $\mathbf{1}^{ox}$ can be interconverted through the addition of O_2 or Et_4NOH (Scheme 2, step G). Hydroxide ions have for a long time been known to induce the reduction of some compounds.[24a] In neutral tris(dithiolene), complexes of molybdenum(VI) (and also tungsten(VI)) are reduced to Mo(V) under the influence of Bu_4NOH, via HO^- coordination and S−Mo bond expansion at the molybdenum center.[24b] In addition, Tolman and co-workers[24c] invoked a similar reactive species like [LCu(III)(OH)] complex which reacts with dihydroanthracene to yield anthracene and

dx.doi.org/10.1021/ic501742j | Inorg. Chem. 2014, 53, 12799−12808

[LCu(II)(OH_2)] complex. In the light of these observations, we can propose the formation of a hydroxide adduct as intermediate for the reduction of $\mathbf{1}^{ox}$ to $\mathbf{1}^{red}$ in the presence of Et_4NOH (Scheme 3). We refrain at this stage from speculating more about mechanistic aspects of the $\mathbf{1}^{ox}/\mathbf{1}^{red}$ redox process.

Scheme 3. Proposed Pathway for the Interconversion between $\mathbf{1}^{ox}$ and $\mathbf{1}^{red}$[a]

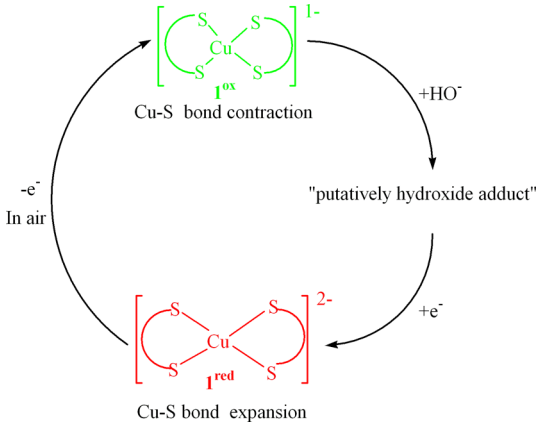

[a]In the presence of Et_4NOH, putatively hydroxide adduct facilitates the electronic readjustment across the Cu–S bonds resulting in the formal reduction of the oxidized $\mathbf{1}^{ox}$. The reduced species immediately changed into oxidized form under oxygen.

EPR Spectroscopy. In order to gather more information on the nature and electronic properties of $\mathbf{1}^{red}$, we performed EPR experiments on powder, frozen DMF solution, and oriented single crystal samples. Figure 5A shows the X-band EPR spectrum of a powder sample of $\mathbf{1}^{red}$ at room temperature. Similar spectra (not shown) were obtained in the temperature range of 20–298 K. The simulation of the $\mathbf{1}^{red}$ powder spectrum (Table 2) indicates the presence of a single species, with axial symmetry. When $\mathbf{1}^{red}$ is dissolved in DMF, in the absence of dioxygen, a similar axial signal is observed, but considerably sharper, which allows the visualization of the hyperfine structure of the $g_\perp$ feature (Figure 5B; similar spectra (not shown) were obtained at 20, 50, and 120 K). The EPR spectra of $\mathbf{1}^{red}$ in both powder and frozen solution were satisfactorily simulated assuming similar axially symmetric collinear g- and A-tensors (Table 2), indicating that the solid state structure of $\mathbf{1}^{red}$ is kept in DMF solution. The line widths of the EPR signal are lower in frozen solution due to the absence of dipole–dipole interactions, which are not completely negligible in the solid state. The EPR parameters obtained, $g_\parallel = 2.087$ and $A_\parallel = 170 \times 10^{-4}$ cm^{-1} (Table 2), are in agreement with the Peisach–Blumberg diagram prediction for a complex of Cu(II) coordinated by four sulfur atoms in square planar coordination.[25] Besides the $g_\parallel$ value, also the low $g_\perp$ value is characteristic of Cu(II)–sulfur complexes.[26−29] $\mathbf{1}^{ox}$ showed no EPR signals under the perpendicular mode conditions used throughout this work, as expected for a Cu(III) complex (d^8, $S = 1$; spectra under parallel mode were not acquired). The conversion of $\mathbf{1}^{ox}$ into $\mathbf{1}^{red}$ was also followed by EPR spectroscopy. Addition of Et_4NOH to $\mathbf{1}^{ox}$ in DMF solution changed the spectrum from a nonsignal spectrum to the spectrum characteristic of $\mathbf{1}^{red}$ (i.e., to a spectrum equal to the one in Figure 5B).

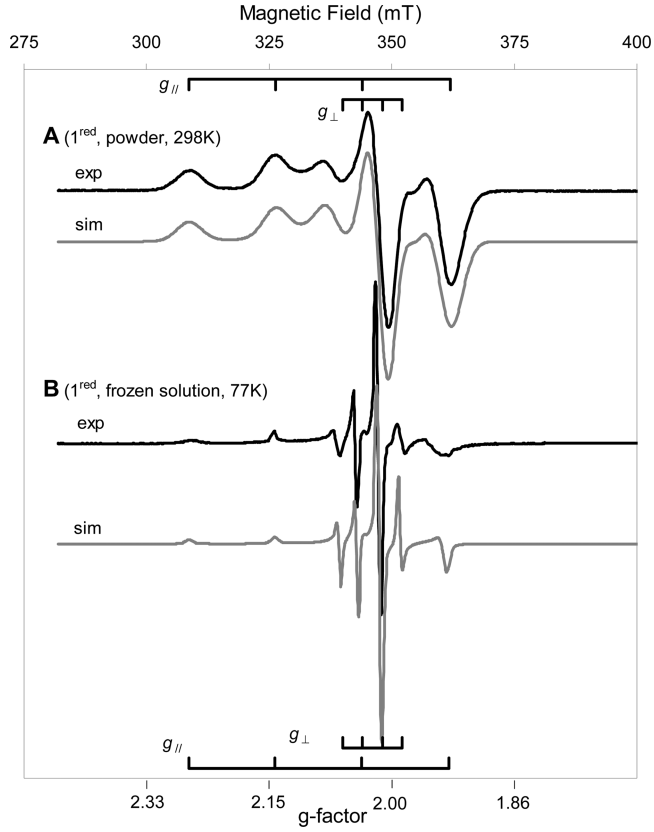

Figure 5. X-band (9.65 GHz) EPR spectra of $\mathbf{1}^{red}$. (A) Powder spectrum at room temperature (298 K); experimental (exp, dark line) and simulation (sim, gray line). (B) Frozen DMF solution (0.15 M of $\mathbf{1}^{red}$) spectrum at 77 K; experimental (exp, dark line) and simulation (sim, gray line). Spectra were acquired as described in the Experimental Section, and the other conditions were as follows: modulation frequency, 100 kHz; modulation amplitude, 0.2 mT; microwave power, 635 μW. Spectra were simulated as indicated in the Experimental Section, with the parameters summarized in Table 2.

Table 2. EPR Parameters of $\mathbf{1}^{red}$

sample	g values (line width (mT))		A values (10^{-4} cm^{-1}) (A values (mT))	
powder	$g_\perp = 2.021$ (4.5)	$g_\parallel = 2.087$ (4.5)	$A_\perp = 38$ (4.0)	$A_\parallel = 170$ (17.4)
soln (in DMF at 0.15 M)	$g_\perp = 2.021$ (0.7)	$g_\parallel = 2.087$ (1.3)	$A_\perp = 38$ (4.0)	$A_\parallel = 167$ (17.2)
single crystal[a]	$g_{1,2,3} = 2.012, 2.016, 2.081$		$A_{1,2,3} = 23, 56, 169$	

[a]Single crystal parameters correspond to Q-band measurements. Eigenvectors are given in the Supporting Information.

Single crystal EPR spectra at both X- and Q-band were taken in three orthogonal planes, as explained in the Experimental Section (see also the Supporting Information for details). As $\mathbf{1}^{red}$ crystallizes in the monoclinic space group $P21/n$, there are two identical copper centers related by a C2b symmetry operation in the unit cell. The symmetry related copper centers are magnetically equivalent for magnetic field orientations lying on the zx plane and along the b crystal axis, but not for any other magnetic field orientations. Figure 6 shows single crystal EPR spectra for selected magnetic field orientations. The spectrum taken along the x axis clearly shows four hyperfine resonance lines, typical of an $S = 1/2$ spin coupled to an $I = 3/2$

dx.doi.org/10.1021/ic501742j | Inorg. Chem. 2014, 53, 12799–12808

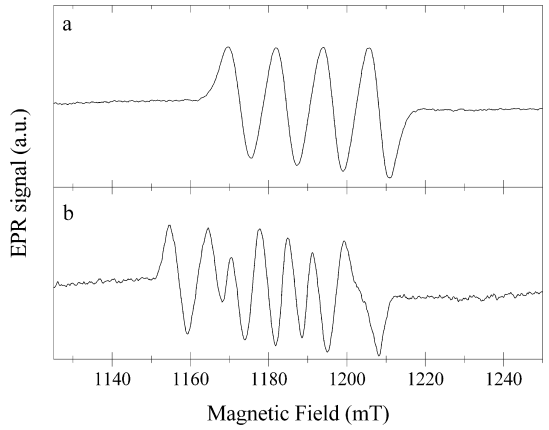

Figure 6. Q-band single crystal EPR spectra of $\mathbf{1}^{red}$ for selected magnetic field orientations: (a) magnetic field along the *x* axis in the *zx* plane; (b) magnetic field at 94° from the *x* axis in the *xy* plane.

nuclear spin (spectrum a). A four-component spectrum with the same separation was obtained at X-band, confirming our assumption that the multiplet spectrum corresponds to hyperfine structure, since it is not microwave frequency dependent. Spectrum b, taken at 94° from the *x* axis in the *xy* plane, shows in contrast eight hyperfine components, as expected for two magnetically nonequivalent identical copper sites. The fact that a nondiluted copper compound shows EPR spectra with well-resolved hyperfine structure was an unexpected result and indicates the presence of very weak exchange and dipolar interactions. This finding is reasonable considering the long distance between copper centers (~11 Å) and the fact that no relevant superexchange pathways are present in the lattice.[30] A similar result was observed for the compound $[N\{n\text{-}Bu)_4]_2[Cu\{mnt)_2]$ studied by Plumlee et al.[31]

The single crystal EPR spectra were least-squares fitted to one or two groups of four equidistant Gaussian shaped resonance lines to evaluate the **g**-and **A**-tensors associated with the copper center.[30] The angular variation of $\mathbf{g}^2$ ($g^2(\theta,\phi)$) and K^2g^2 ($K = ag\mu_B$, where *a* is the hyperfine splitting) at Q-band is shown in Figure S4 in Supporting Information.[32] Similar results were obtained at X-band (not shown). The components of **g**- and **A**-tensors (Table 2 and Table S1 in the Supporting Information) show that the **g**-tensor is roughly axial with the g_1-eigenvector lying approximately along the normal to the equatorial copper ligand plane (Figure S4 in the Supporting Information), and that the eigenvectors of the **g**- and **A**-tensors are nearly coincident. The **g**- and **A**-tensors are typical for Cu(II) ions with four S-ligands in square planar coordination[33] and are compatible with the **g**-and **A**-tensors assumed in the simulation of the powder and frozen solution EPR spectra (Figure 5).

The EPR experiments on powder, frozen solution, and single crystal show that the $\mathbf{1}^{red}$ complex EPR parameters are the ones typical for a four sulfur-coordinated Cu(II) complex. The square-planar geometry observed by X-ray crystallography is in line with the ratio $g_{\|}/A_{\|}$ of 123 cm^{-1}, as this empirical value rises with increasing tetrahedral distortion (square planar structures display values of 105−135 cm^{-1}).[27,34] Moreover, and most important even, the determined EPR parameters indicate a strong covalency for the Cu(II)−S bonds. The delocalized spin density over the complex, which is controlled by the energy levels of the molecular orbitals of the compound, can be evaluated by EPR spectroscopy, using the conventional perturbation approach developed for square planar d^9 systems.[35−39] In fact, several authors have used *g* and *A* values to evaluate the different ratios of σ and π bonding to the metal.[29,35,36,40−42] The fact that $g_{\|} > g_{\perp}$ and $|A_{\|}| > |A_{\perp}|$ indicates a b_{1g} ground state,[35,36] in which case the *A* values of an

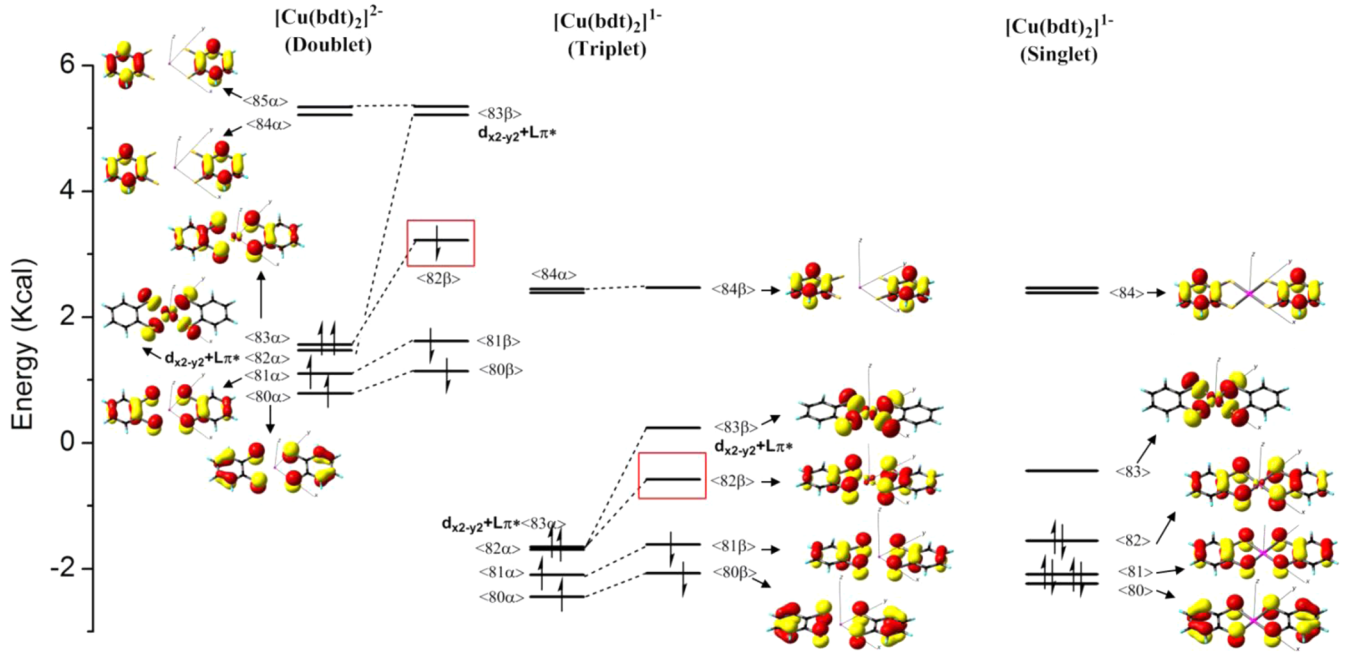

Figure 7. Molecular orbital diagram for the electron transfer process in $\mathbf{1}^{red}/\mathbf{1}^{ox}$ ($[Cu(bdt)_2]^{2-}$ doublet in left, the putatively $[Cu(bdt)_2]^{1-}$ triplet in middle, $[Cu(bdt)_2]^{1-}$ singlet in right). Selected MOs are shown. Red box indicates the removal of one electron from HOMO during the oxidation process.

dx.doi.org/10.1021/ic501742j | *Inorg. Chem.* 2014, 53, 12799−12808

unpaired electron in such orbital can be interpreted by eqs 1 and 2,[35,36]

$$A_{\parallel} = P[-\kappa - (4/7)\alpha^2 + \Delta g_{\parallel} + (3/7)\Delta g_{\perp}] \quad (1)$$

$$A_{\perp} = P[-\kappa + (2/7)\alpha^2 + (11/14)\Delta g_{\perp}] \quad (2)$$

where P is the dipolar hyperfine coupling constant of the unpaired electron ($P = \beta_e g_e \beta_N g_N \langle r^{-3} \rangle = 0.0388$ cm^{-1}),[43] κ is a factor related to the isotropic hyperfine coupling constant, $\Delta g_{\parallel} = g_{\parallel} - 2.0023$, $\Delta g_{\perp} = g_{\perp} - 2.0023$, and α is the coefficient of the $d_{x^2-y^2}$ orbital of b_{1g}. The α^2, which can be interpreted as a "covalency" parameter, describes the in-plane metal−ligand σ bonding. It is equal to 1, for pure ionic bonding, and <1, for covalent bonding.[35,44] Assuming negative signs for $A_{\parallel}$ and $A_{\perp}$ (because positive A values originate α and κ unrealistic values, as found by others[40,41]), α^2 was found to be 0.510 and κ to be 0.257. Similar α^2 values can be determined in other copper−sulfur complexes.[27,45,46] Moreover, the α^2 value of 0.5 is within the limits calculated by Hoffmann et al.[29] for square-planar copper−sulfur complexes The low α^2 value of $\mathbf{1}^{red}$ indicates a large delocalization of the unpaired electron density onto the sulfur atoms, as it was suggested for other $\{CuS_4\}$ complexes.[27,29,45,46]

DFT Calculations. To understand the electronic structure of the synthesized complex $\mathbf{1}^{red}$, and support the strong covalency of its Cu−S bonds revealed by the EPR experiments, we have carried out DFT calculations.[12] A qualitative MO diagram is shown in Figure 7. Open shell doublet geometry optimization followed by single point calculation on $\mathbf{1}^{red}$ indicates that both HOMO (highest occupied molecular orbital) (82β) and LUMO (lowest occupied molecular orbital) (83β) are beta spinator. LUMO is originated by antibonding interaction of S−π and metal d orbital (bonding part is deeply buried). SOMO (single occupied molecular orbital) is a beta counter orbital of LUMO and shows that the spin density is 76% delocalized on the four sulfur atoms (each ∼19%) and 24% on the copper atom. This spin delocalization is in qualitative agreement with the covalency determined by the experimental EPR parameters ($\alpha^2 \approx 0.5$), which suggested that ≈50% of the spin population is in the copper $d_{x^2-y^2}$ orbital. Although the numeric difference between the calculated and experimental values is considerable, a similar high discrepancy was observed by Finazzo et al.,[41] who reported spin delocalization values in copper phthalocyanine complexes of ≈75 and ≈58%, based on EPR and DFT data, respectively. These discrepancies have been attributed to an overestimation of the covalency or to deficiencies of the available DFT functionals.[41,42,47−51] Nevertheless, the DFT results support the experimentally observed trend. Based on our EPR (experimental) and DFT (theoretical) results, the unpaired electron of $\mathbf{1}^{red}$ is highly delocalized on the four sulfur atoms, suggesting a significant radical character on the sulfur atoms ("thiyl radical character"). The TD-DFT calculation (see the Supporting Information) identified such ligand to ligand charge transfer (LLCT) transition at 425.14 nm, and the computed electronic spectra for both $\mathbf{1}^{ox}$ and $\mathbf{1}^{red}$ are presented in Figure 3B. Thus, the reduced species is unique and $\mathbf{1}^{red}$ is better described by the two isoelectronic structures $[Cu^{I}(bdt_2, 4S^{3-\bullet})]^{2-} \leftrightarrow [Cu^{II}(bdt_2, 4S^{4-})]^{2-}$, with the square-planar structure being stabilized by delocalization of the unpaired electron over 5 atoms, 4 sulfurs, and 1 copper. A similar situation was described for compounds of the type $[(L_2Cu)_3, S_2]^{3+}$.[52]

The electronic structure of the one electron oxidation of $\mathbf{1}^{red}$ has also been explored. The redox traces of the cyclic voltammograms correlate well with the DFT results, and the process of oxidation of $\mathbf{1}^{red}$ can be described as the removal of one electron from HOMO (82β, Sπ orbital; Figure 7 left, red box) to form the stable singlet $[Cu(bdt)_2]^{1-}$. This oxidation required 4.27 eV, which corresponds to the calculated $E_{1/2}$ = −0.27 V vs SHE. In such electron transfer the existence of a putatively triplet $[Cu(bdt)_2]^{1-}$ intermediate with two unpaired electrons located mostly on ligand Sπ (Figure 8) may respond

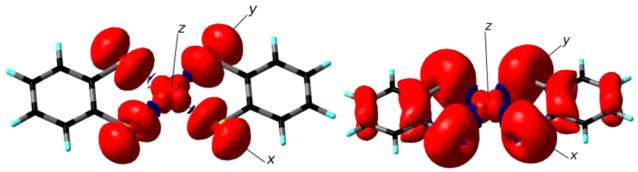

Figure 8. Mulliken spin density of $[Cu(bdt)_2]^{2-}$ (doublet) in left and $[Cu(bdt)_2]^{1-}$ (triplet) in right.

to a rapid spin rearrangement to form the stable singlet $[Cu(bdt)_2]^{1-}$, which is in agreement with others previously reported.[6,53] The oxidation process is schematized in Scheme 4.

Scheme 4. Proposed Pathway for the One Electron Oxidation of $\mathbf{1}^{red}$ to $\mathbf{1}^{ox}$

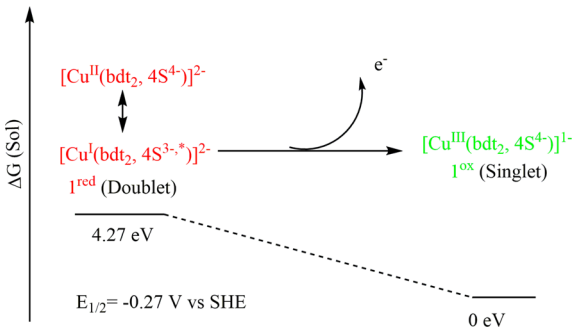

The $\mathbf{1}^{red}$ electronic structure description as $[Cu^{I}(bdt_2, (4S^{3-\bullet})]^{2-}$ may explain its aerial oxidation to a putatively intermediate triplet state, $[Cu^{I}(bdt_2, 4S^{2-\bullet\bullet})]^{1-}$ that rapidly changes to acquire the singlet electronic state, $[Cu^{III}(bdt_2, 4S^{4-})]^{1-}$, as was suggested by Wieghardt.[6] As oxidation by one electron is coupled with electronic rearrangement without any structural reorganization of the molecule, the oxidative traces of the cyclic voltammograms would be expected to be reversible.

CONCLUSIONS

The synthesis of the one electron reduced form of the $\mathbf{1}^{ox}$ complex was long overdue. Now we have synthesized it in the solid state and structurally characterized and spectroscopically identified the $[Ph_4P]_2[Cu(bdt)_2]$ complex ($\mathbf{1}^{red}$, Figure 1). $\mathbf{1}^{red}$ is highly prone toward dioxygen, yielding the one electron oxidized compound $[Ph_4P][Cu(bdt)_2]$ ($\mathbf{1}^{ox}$). However, as shown by cyclic voltammetry, UV−visible titration, and EPR experiments, the two complexes are easily interconverted, and $\mathbf{1}^{red}$ can be re-formed from $\mathbf{1}^{ox}$ in the presence of Et_4NOH. EPR experiments showed that $\mathbf{1}^{red}$ is a Cu(II)−sulfur complex and revealed covalent Cu−S bonds. DFT calculations confirmed this high electron density on the sulfur atoms, providing an estimate of 19% of the unpaired spin on each

dx.doi.org/10.1021/ic501742j | Inorg. Chem. 2014, 53, 12799−12808

sulfur atom (total of 76%) and of 24% on the copper atom, thus suggesting that $\mathbf{1}^{red}$ has a "thiyl radical character". Such radical character leads to LLCT transition as computed by TD-DFT. More importantly, its consensus electronic structure derived from its spectroscopic data and DFT calculations should be considered as the resonance forms of $[Cu^{II}(bdt_2, 4S^{4-}]^{2-} \leftrightarrow [Cu^{I}(bdt_2, 4S^{3-\bullet})]^{2-}$ species in which thiyl radical is delocalized over four sulfur atoms via Cu−S bond interaction. Oxidation of $\mathbf{1}^{red}$ (doublet state) was proposed to lead to a possible triplet state that eventually stabilized into a $\mathbf{1}^{ox}$ singlet state, $[Cu^{III}(bdt_2,4S^{4-})]^{1-}$. Taken together, our results provide new insights into the coordination chemistry of transition metal ions in sulfur rich environments. In particular, a switching mechanism between distinct oxidation states ($\mathbf{1}^{red}$ and $\mathbf{1}^{ox}$) was discussed. The present work highlights the interplay between electronic structure, covalency, and redox events occurring in copper ions in sulfur rich environments.

■ ASSOCIATED CONTENT

Ⓢ Supporting Information

Additional UV−visible, EPR data, optimized *xyz* coordinates for all (DFT), TD-DFT data, and cif file of $\mathbf{1}^{red}$. This material is available free of charge via the Internet at http://pubs.acs.org.

■ AUTHOR INFORMATION

Corresponding Authors

*E-mail: jose.moura@fct.unl.pt (J.J.G.M.).
*E-mail: teresa.aviles@fct.unl.pt (T.A.).
*E-mail: brondino@fbcb.unl.edu.ar (C.D.B.).
*E-mail: abya@iitk.ac.in (S.S.).

Present Address

⊥LAQV@REQUIMTE, Departamento Química, Faculdade de Ciências e Tecnologia, Universidade Nova de Lisboa, 2829-516 Caparica, Portugal.

Notes

The authors declare no competing financial interest.

■ ACKNOWLEDGMENTS

This work was supported by FCT/MEC-Portugal (SFRH/BPD/63066/2009, PTDC/QUI-BIQ/098071/2008, PTDC/QUI-QUI/099873/2008, FCT-ANR/BBB-MET0023/2012, and PEst-C/EQB/LA0006/2013) in Portugal; by UNL (CAID-PI 11058), CONICET (PIP 2014GI), and MINCYT (PICT 2011-1654) in Argentina; and by SERB-DST (SR/S1/RFIC-01/2011) and CSIR (SRF) in New Delhi, India. S.R.P. is an IF FCT fellow.

■ REFERENCES

(1) Gray, H. B.; Billig, E. *J. Am. Chem. Soc.* **1963**, *85*, 2019. Baker-Hawkes, M. J.; Billig, E.; Gray, H. B. *J. Am. Chem. Soc.* **1966**, *88*, 4870. Bachler, V.; Olbrich, G.; Neese, F.; Wieghardt, K. *Inorg. Chem.* **2002**, *41*, 4179. *Progress in Inorganic Chemistry*; Stiefel, E. I., Ed.; Wiley: 2003; Vol. *52*, p 1. Benedito, F. L.; Petrenko, T.; Bill, E.; Weyhermuller, T.; Wieghardt, K. *Inorg. Chem.* **2009**, *48*, 10913. Eisenberg, R.; Gray, H. B. *Inorg. Chem.* **2011**, *50*, 9741. Sproules, S.; Wieghardt, K. *Coord. Chem. Rev.* **2011**, *255*, 837. McNamara, W. R.; Han, Z.; Yin, C.-J.; Brennesse, W. W.; Holland, P. L.; Eisenberg, R. *Proc. Natl. Acad. Sci. U.S.A.* **2012**, *109*, 15594. Letko, C. S.; Panetier, J. A.; Head-Gordon, M.; Tilley, T. D. *J. Am. Chem. Soc.* **2014**, *136*, 9364. Fang, M.; Engelhard, M. H.; Zhu, Z.; Helm, M. L.; Roberts, J. A.S. *ACS Catal.* **2014**, *4*, 90.

(2) Stiefel, E. I.; Waters, J. H.; Billig, E.; Gray, H. B. *J. Am. Chem. Soc.* **1965**, *87*, 3016. Sellmann, D.; Binder, H.; Haeusinger, D.; Heinemann, F. W.; Sutter, J. *Inorg. Chim. Acta* **2000**, *829*, 300.

(3) Rajagopalan, K. V.; Johnson, J. L. *J. Biol. Chem.* **1992**, *267*, 10199. Hille, R. *Dalton Trans.* **2013**, *42*, 3029.

(4) Mrkvová, K.; Kamenícek, J.; Sindelar, Z.; Kvítek, L.; Mrozinski, J.; Nahorska, M.; Zak, Z. *Transition Met. Chem.* **2004**, *29*, 238.

(5) Sawyer, D. T.; Srivatsa, G. S.; Bodini, M. E.; Schaefer, W. P.; Wing, R. M. *J. Am. Chem. Soc.* **1986**, *108*, 936.

(6) Ray, K.; Weyhermu1ller, T.; Neese, F.; Wieghardt, K. *Inorg. Chem.* **2005**, *44*, 5345.

(7) Maiti, B. K.; Pal, K.; Sarkar, S. *Inorg. Chem. Commun.* **2004**, *7*, 1027.

(8) Sheldrick, G. M. *SADABS, Program for Siemens area detector absorption correction*; University of Göttingen: Göttingen, Germany, 1996.

(9) Sheldrick, G. M. SHELXS97, A Program for the Solution of Crystal Structures from X-ray Data, University of Göttingen, Germany, 1997; Sheldrick, G. M. SHELXL97, A Program for the Refinement of Crystal Structures from X-ray Data, University of Göttingen, Germany, 1997.

(10) Spek, A. L. *PLATON*: University of Utrecht: Utrecht, The Netherlands, 2001. Spek, A. L. *Acta Crystallogr.* **1990**, *4*, 194.

(11) Schveigkardt, J. M.; Rizzi, A. C.; Piro, O. E.; Castellano, E. E.; Santana, R. C. D.; Calvo, R.; Brondino, C. D. *Eur. J. Inorg. Chem.* **2002**, 2913.

(12) Frisch, M. J.; Trucks, G. W.; Schlegel, H. B.; Scuseria, G. E.;Robb, M. A.; Cheeseman, J. R.; Montgomery, J. A.; Vreven, T., Jr.; Kudin, K. N.; Burant, J. C.; Millam, J. M.; Iyengar, S. S.; Tomasi, J.; Barone, V.; Mennucci, B.; Cossi, M.; Scalmani, G.; Rega, N.; Petersson, G. A.; Nakatsuji, H.; Hada, M.; Ehara, M.; Toyota, K.; Fukuda, R.; Hasegawa, J.; Ishida, M.; Nakajima, T.; Honda, Y.; Kitao, O.; Nakai, H.; Klene, M.; Li, X.; Knox, J. E.; Hratchian, H. P.; Cross, J. B.; Bakken, V.; Adamo, C.; Jaramillo, J.; Gomperts, R.; Stratmann, R. E.; Yazyev, O.; Austin, A. J.; Cammi, R.; Pomelli, C.; Ochterski, J. W.; Ayala, P. Y.; Morokuma, K.; Voth, G. A.; Salvador, P.; Dannenberg, J. J.; Zakrzewski, V. G.; Dapprich, S.; Daniels, A. D.; Strain, M. C.; Farkas, O.; Malick, D. K.; Rabuck, A. D.; Raghavachari, K.; Foresman, J. B.; Ortiz, J. V.; Cui, Q.; Baboul, A. G.; Clifford, S.; Cioslowski, J.; Stefanov, B. B.; Liu, G.; Liashenko, A.; Piskorz, P.; Komaromi, I.; Martin, R. L.; Fox, D. J.; Keith, T.; Al-Laham, M. A.; Peng, C. Y.; Nanayakkara, A.; Challacombe, M.; Gill, P. M. W.; Johnson, B.; Chen, W.; Wong, M. W.; Gonzalez, C. ; Pople, J. A. *GAUSSIAN 03 (Revision B.04)*; Gaussian, Inc.: Pittsburgh, PA, 2003.

(13) Becke, D. *J. Chem. Phys.* **1993**, *98*, 5648.

(14) Petersson, G. A.; Al-Laham, M. A. *J. Chem. Phys.* **1991**, *94*, 6081.

(15) Hay, P. J.; Wadt, W. R. *J. Chem. Phys.* **1985**, *82*, 299.

(16) Hay, P. J.; Wadt, W. R. *J. Chem. Phys.* **1985**, *82*, 270.

(17) (a) Smith, P. E.; Brunne, R. M.; Mark, A. E.; Gunsteren, W. F. *J. Phys. Chem.* **1993**, *97*, 2009−2014. (b) Löffler, G.; Schreiber, H.; Steinhauser, O. *J. Mol. Biol.* **1997**, *270*, 520−534. (c) Ogliaro, F.; de Visser, S. P.; Cohen, S.; Sharma, P. K.; Shaik, S. *J. Am. Chem. Soc.* **2002**, *124*, 2806−2814.

(18) Reiss, H.; Heller, A. *J. Phys. Chem.* **1985**, *89*, 4207.

(19) Maiti, B. K.; Avilés, T.; Matzapetakis, M.; Moura, I.; Pauleta, S. R.; Moura, J. J. G. *Eur. J. Inorg. Chem.* **2012**, 4159. Maiti, B. K.; Avilés, T.; Moura, I.; Pauleta, S. R.; Moura, J. J. G. *Inorg. Chem. Commun.* **2014**, *45*, 97.

(20) George, G. N.; Pickering, I. J.; Yu, Y. E.; Prince, R. C.; Bursakov, S. A.; Gavel, O. Y.; Moura, I.; Moura, J. J. G. *J. Am. Chem. Soc.* **2000**, *122*, 8321. Bursakov, S. A.; Gavel, O. Yu.; Di Rocco, G.; Lampreia, J.; Calvete, J.; Pereira, A. S.; Moura, J. J. G.; Moura, I. *J. Inorg. Biochem.* **2004**, *98*, 833.

(21) Bose, M.; Moula, G.; Begum, A.; Sarkar, S. *Inorg. Chem.* **2011**, *50*, 3852.

(22) Sarkar, S.; Mishra, S. B. S. *Coord. Chem. Rev.* **1984**, *59*, 239. Chandrasekaran, J.; Ansari, M. A.; Sarkar, S. *J. Less-Common Met.* **1987**, *134*, L23. Ansari, M. A.; Chandrasekaran, J.; Sarkar, S. *Inorg. Chem.* **1988**, *27*, 763.

(23) Sarangi, R.; George, S. D.; Rudd, D. J.; Szilagyi, R. K.; Ribas, X.; Rovira, C.; Almeida, M.; Hodgson, K. O.; Hedman, B.; Solomon, E. I. *J. Am. Chem. Soc.* **2007**, *129*, 2316. Hanss, J.; Kröger, H. J. *Angew.*

Chem., Int. Ed. **1998**, *37*, 360. Leut, A.; Armstrong, D. A. *J. Phys. Chem.* **1986**, *90*, 1449.
(24) (a) Sawyer, D. T.; Roberts, J. L., Jr. *Acc. Chem. Res.* **1988**, *21*, 469. (b) Cervilla, A.; Pérez-Plá, F.; Llopis, E.; Piles, M. *Dalton Trans.* **2004**, 1461. (c) Donoghue, P. J.; Tehranchi, J.; Cramer, C. J.; Sarangi, R.; Solomon, E. I.; Tolman, W. B. *J. Am. Chem. Soc.* **2011**, *133*, 17602.
(25) Peisach, J.; Blumberg, W. E. *Arch. Biochem. Biophys.* **1974**, *165*, 691.
(26) Nishida, Y.; Kida, S. *Coord. Chem. Rev.* **1979**, *27*, 275.
(27) Sakaguchi, U.; Addison, A. W. *J. Chem. Soc., Dalton Trans.* **1979**, 600.
(28) Symons, M. C. R.; West, D. X. *J. Chem. Soc., Dalton Trans.* **1985**, 379.
(29) Hoffmann, S. K.; Goslar, J.; Lijewski, S.; Zalewska, A. *J. Magn. Reson.* **2013**, *236*, 7.
(30) Neuman, N. I.; Perec, M.; González, P. J.; Passeggi, M. C. G.; Rizzi, A. C.; Brondino, C. D. *J. Phys. Chem. A* **2010**, *114*, 13069.
(31) Plumlee, K. W.; Hoffman, B. M.; Ibers, J. A. *J. Chem. Phys.* **1975**, *63*, 1926.
(32) Weil, J. A.; Bolton, J. R. *Electron Paramagnetic Resonance*, 2nd ed.; John Wiley & Sons, Inc.: Hoboken, NJ, 2007.
(33) Brondino, C. D.; Casado, N. M. C.; Passeggi, M. C. C.; Calvo, R. *Inorg. Chem.* **1993**, *32*, 2078.
(34) Yokoi, H.; Addison, A. W. *Inorg. Chem.* **1977**, *16*, 1341.
(35) Maki, A. H.; McGarvey, B. R. *J. Chem. Phys.* **1958**, *29*, 31.
(36) Maki, A. H.; McGarvey, B. R. *J. Chem. Phys.* **1958**, *29*, 35.
(37) Gersmann, H. G.; Swalen, J. D. *J. Chem. Phys.* **1962**, *36*, 3221.
(38) Neiman, R.; Kivelson, D. *J. Chem. Phys.* **1962**, *35*, 149.
(39) McGarvey, B. R. *J. Phys. Chem.* **1967**, *71*, 51.
(40) Valente, M.; Freire, C.; Castro, B. *J. Chem. Soc., Dalton Trans.* **1998**, 1557.
(41) Finazzo, C.; Calle, C.; Stoll, S.; Doorslaer, S. V.; Schweiger, A. *Phys. Chem. Chem. Phys.* **2006**, *8*, 1942.
(42) Moons, H.; Łapok, Ł.; Loas, A.; Doorslaer, S. V.; Gorun, S. M. *Inorg. Chem.* **2010**, *49*, 8779.
(43) Maroney, M. J.; Norman, J. G.; Osborne, J. H. *Inorg. Chem.* **1984**, *23*, 2261.
(44) Rockenbauer, A. *J. Magn. Reson.* **1979**, *35*, 429.
(45) Haiduc, I.; David, L.; Cozar, O.; Micu-Semeniuc, R.; Mezei, G.; Armenean, M. *J. Mol. Struct.* **1999**, *482*, 153.
(46) Fabretti, A. C.; Ferrari, M.; Franchini, G. C.; Giusto, A.; Preti, C.; Tosi, G. *Transition Metal Chem.* **1989**, *8*, 8.
(47) Solomon, E. I.; Szilagyi, R. K.; DeBeer, S.; Basumallick, L. *Chem. Rev.* **2004**, *104*, 419.
(48) Sinnecker, S.; Neese, F. *J. Comput. Chem.* **2006**, *27*, 1463.
(49) Remenyi, C.; Reviakine, R.; Kaupp, M. *J. Phys. Chem. B* **2007**, *111*, 8290.
(50) Neese, F. *Coord. Chem. Rev.* **2009**, *253*, 526.
(51) Zhekova, H. R.; Seth, M.; Ziegler, T. *J. Phys. Chem. A* **2010**, *114*, 6308.
(52) Vidossich, P.; Lledós, A. *Dalton Trans.* **2014**, *43*, 11145.
(53) Waters, T.; Wang, X.-B.; Woo, H.-K.; Wang, L.-S. *Inorg. Chem.* **2006**, *45*, 5841.